JOURNAL OF Materials CHEMISTRY

Discotic liquid crystals of transition metal complexes. Part 26:† Supramolecular structures of long-chain-substituted octaphenyltetrapyrazinoporphyrazine derivatives

Kazuchika Ohta,*[a] Satoru Azumane,[a] Wataru Kawahara,[a] Nagao Kobayashi[b] and Iwao Yamamoto[a]

[a]*Department of Functional Polymer Science, Faculty of Textile Science and Technology, Shinshu University, 386-8567 Ueda, Japan. E-mail: ko52517@giptc.shinshu-u.ac.jp*
[b]*Department of Chemistry, Graduate School of Science, Tohoku University, Sendai 980-8578, Japan*

Received 8th July 1999, Accepted 28th July 1999

Ten novel columnar liquid crystals, [octakis(4-alkoxyphenyl)tetrapyrazinoporphyrazinato]metal(II) (abbreviated as $(C_nO)_8$–M; $n=10$, 12; M = Cu, Ni) and [octakis(3,4-dialkoxyphenyl)tetrapyrazinoporphyrazinato]metal(II) (abbreviated as $(C_nO)_{16}$–M; $n=8$, 10, 12; M = Cu, Ni), have been synthesized and characterized. It was found that the mesophase structures of $(C_nO)_8$–M are very sensitive to the central metal and closely related to the aggregate structures in the solution. The $(C_nO)_{16}$–M derivatives exhibit a D_{hd} mesophase at lower temperatures and a D_{rd} (*C*2/*m*) phase at higher temperatures. Thus, the mesophase with higher symmetry appears at lower temperatures for these $(C_nO)_{16}$–M derivatives. This is quite opposite to the general tendency for the higher symmetry mesophase to appear at higher temperatures. In order to further clarify the structures of both the mesophases and the aggregate in solutions, the electronic and magnetic circular dichromism (MCD) spectra were measured. The Q band of $(C_nO)_{16}$–M in *n*-hexane showed a wide Davidov splitting. It was proven that such a wide splitting of the Q band can be attributed to the formation of dimers. The dimerization was confirmed by vapor pressure osmometric (VPO) measurements in *n*-hexane solution. Furthermore, the spectrum of the thin film in the mesophase in the absence of solvent at room temperature was similar to that of the *n*-hexane solution. From these electronic absorption spectra, MCD spectra, VPO measurements and temperature-dependent X-ray diffraction studies, it was clarified for $(C_nO)_{16}$–M that the dimer structure in *n*-hexane solution is closely related to those in the thermotropic mesophases.

1 Introduction

In general, if a very small amount of compound is added into a pure solvent, each of the solute molecules is completely separated from the others. When the concentration is gradually increased, one molecule comes closer to another molecule to form a dimer. Upon further elevating the concentration, they stepwise form a trimer, tetramer, ..., oligomer, and finally multimer in this fluid solution. When the concentration is infinitely elevated; in other words, when the system becomes a pure compound without a solvent, it shows a thermotropic liquid-crystalline state in some cases. This thermotropic liquid-crystalline phase may have a structure that is very similar to those of the preceding aggregation states. In this work, we reveal that our synthesized metal complexes $(C_nO)_{16}$–M form dimers in non-polar solvents, and that this dimer becomes a unit disk in a thermotropic hexagonal columnar mesophase in the absence of solvent. Hence, the analysis of aggregate structure in solution is very useful for the analysis of pure thermotropic mesophase structure. We believe that the present example of dimer-forming liquid-crystalline complexes will contribute to the fields of both solution chemistry and liquid crystal chemistry.

2 Experimental

Measurements

Precursors, 2,3-dicyano-5,6-bis(3,4-dialkoxyphenyl)pyrazine derivatives, were identified by using a JEOL A100 infrared spectrometer and a JEOL JNM PMX60si (60 MHz) NMR spectrometer. Final products were identified by elemental analysis (Table 1) and electronic absorption spectra (Table 2) using a Perkin Elemental Analyzer 240B and a Hitachi 330 spectrometer, respectively. The phase transition behavior of these compounds was observed by using a polarizing microscope (Olympus BH-2) equipped with a heating plate controlled by a thermoregulator (Mettler FP80 and FP82) and measured with a differential scanning calorimeter (Shimadzu DSC-50). Temperature-dependent X-ray diffraction measurements of the mesophases were performed by using a Rigaku Geigerflex with Cu-Kα radiation equipped with a hand-made heating plate controlled by a thermoregulater.[2] Temperature-dependent electronic spectra were recorded by the technique reported in our previous paper.[2b]

Synthesis

The synthetic routes to the $(C_nO)_8$–M (M = Cu **1**, M = Ni **2**) and $(C_nO)_{16}$–M (M = Cu **3**, M = Ni **4**) derivatives are shown in Fig. 1. Precursors **5** and **7** were synthesized from the purchased raw materials according to our previously reported method.[3] The detailed procedures are described for a representative 4-dodecyloxy dicyanopyrazine derivative (**6c**) and the corresponding $(C_{12}O)_8$–Cu (**1**) in the following section; the other derivatives were synthesized in the same manner. In Table 1 are summarized the elemental analysis data of the $(C_nO)_8$–M and $(C_nO)_{16}$–M complexes. Electronic absorption spectral data of these complexes are listed in Table 2.

2,3-Dicyano-5,6-bis(4-dodecyloxyphenyl)pyrazine 6c. The pyrazine derivative **6c** was prepared by Kanakarajan's

†Part 25: Ref. 1.

Table 1 Elemental analysis data of $(C_nO)_8$–M (M = Cu **1**, M = Ni **2**) and $(C_nO)_{16}$–M (M = Cu **3**, M = Ni **4**)

		Found (calc.) (%)		
Complex	Molecular formula (*M*)	C	H	N
1b: $(C_{10}O)_8$–Cu	$C_{152}H_{200}N_{16}O_8Cu$ (2442.93)	74.01 (74.73)	8.30 (8.25)	9.20 (9.17)
1c: $(C_{12}O)_8$–Cu	$C_{168}H_{232}N_{16}O_8Cu$ (2667.36)	75.17 (75.65)	8.76 (8.77)	8.16 (8.40)
2b: $(C_{10}O)_8$–Ni	$C_{152}H_{200}N_{16}O_8Ni$ (2438.08)	75.12 (74.88)	8.42 (8.27)	9.20 (9.19)
2c: $(C_{12}O)_8$–Ni	$C_{168}H_{232}N_{16}O_8Ni$ (2662.52)	75.46 (75.79)	8.78 (8.78)	8.23 (8.42)
3a: $(C_8O)_{16}$–Cu	$C_{200}H_{296}N_{16}O_8Cu$ (3244.23)	73.43 (74.05)	9.18 (9.20)	6.85 (6.91)
3b: $(C_{10}O)_{16}$–Cu	$C_{232}H_{360}N_{16}O_8Cu$ (3693.09)	74.25 (75.45)	9.84 (9.83)	6.10 (6.07)
3c: $(C_{12}O)_{16}$–Cu	$C_{264}H_{424}N_{16}O_8Cu$ (4141.95)	76.44 (76.56)	10.32 (10.32)	5.05 (5.41)
4a: $(C_8O)_{16}$–Ni	$C_{200}H_{296}N_{16}O_8Ni$ (3239.58)	73.37 (74.15)	9.10 (9.21)	6.71 (6.92)
4b: $(C_{10}O)_{16}$–Ni	$C_{232}H_{360}N_{16}O_8Ni$ (3688.24)	75.40 (75.55)	9.75 (9.84)	5.82 (6.08)
4c: $(C_{12}O)_{16}$–Ni	$C_{264}H_{424}N_{16}O_8Ni$ (4137.11)	76.51 (76.65)	10.30 (10.33)	5.11 (5.42)

method.[4] A mixture of 4,4′-didodecyloxybenzyl (1.90 g, 3.11 mmol) and diaminomaleonitrile (0.89 g, 7.8 mmol) in 50 ml of acetic acid was refluxed under a nitrogen atmosphere for 10 h. After cooling to room temperature, the crude product was extracted with chloroform and washed with water. The organic layer was dried over anhydrous sodium sulfate and the solvent was removed under reduced pressure using a rotary evaporator. The resulting solid was purified by using column chromatography (SiO_2 gel, benzene : hexane = 5 : 1 (v/v), $R_f = 0.66$) to give 1.66 g of 2,3-dicyano-5,6-bis(4-dodecyloxyphenyl)pyrazine **6c** as a yellow solid. Yield 82%. Mp = 88 °C. ^{1}H NMR ($CDCl_3$, TMS): δ 7.44 (d, 4H, phenyl), 6.75 (d, 4H, phenyl), 3.93 (t, 4H, –CH_2–), 1.25 (m, 40H, –$(CH_2)_{10}$–), 0.87 (t, 6H, –CH_3). IR (KBr): 2940, 2850, 2250, 1600, 1500, 1460 cm^{-1}.

2,3-Dicyano-5,6-bis(4-decyloxyphenyl)pyrazine 6b. Purified by column chromatography (SiO_2 gel, benzene : hexane = 5 : 1 (v/v), $R_f = 0.51$). Yellow solid. Yield 88%. Mp = 78 °C. ^{1}H NMR ($CDCl_3$, TMS): δ 7.40 (d, 4H, phenyl), 6.70 (d, 4H, phenyl), 3.92 (t, 4H, –OCH_2–), 1.28 (m, 32H, –$(CH_2)_8$–), 0.88 (t, 6H, –CH_3). IR (KBr): 2925, 2860, 2240, 1600, 1510, 1460 cm^{-1}.

2,3-Dicyano-5,6-bis(3,4-didodecyloxyphenyl)pyrazine 8c. Purified by column chromatography (SiO_2 gel, benzene : $CHCl_3$ = 5 : 1 (v/v), $R_f = 0.80$). Yellow solid. Yield 85%. Mp = 75 °C. ^{1}H NMR (CCl_4, TMS): δ 7.02–6.52 (m, 6H, phenyl), 3.93 (t, 4H, –OCH_2–), 3.80 (t, 4H, –OCH_2–), 1.24 (m, 80H, –$(CH_2)_{10}$–), 0.87 (t, 12H, –CH_3). IR (KBr): 2920, 2860, 1580, 1490, 1460 cm^{-1}.

2,3-Dicyano-5,6-bis(3,4-didecyloxyphenyl)pyrazine 8b. Purified by chromatography (SiO_2, benzene, $R_f = 0.70$). Yellow solid. Yield 66%. Mp = 66 °C. ^{1}H NMR ($CDCl_3$, TMS): δ 7.13–6.63 (m, 6H, phenyl), 3.93 (t, 4H, –OCH_2–), 3.79 (t, 4H, –OCH_2–), 1.23 (m, 64H, –$(CH_2)_8$–) 0.87 (t, 12H, –CH_3). IR (KBr): 2950, 2860, 2230, 1590, 1500, 1460 cm^{-1}.

2,3-Dicyano-5,6-bis(3,4-dioctyloxyphenyl)pyrazine 8a. Purified by chromatography (SiO_2 gel, benzene, $R_f = 0.55$). Yellow solid. Yield 64%. Mp = 58 °C. ^{1}H NMR ($CDCl_3$, TMS): δ 7.26–6.75 (m, 6H, phenyl), 4.00 (t, 4H, –OCH_2–), 3.83 (t, 4H, –OCH_2–), 1.31 (m, 48H, –$(CH_2)_6$–), 0.89 (t, 12H, –CH_3). IR (KBr): 2950, 2860, 2230, 1590, 1500, 1460 cm^{-1}.

[Octakis(4-dodecyloxyphenyl)tetrapyrazinoporphyrazinato]-copper(II): $(C_{12}O)_8$–Cu 1c. The copper(II) complex **1** was prepared by Tomoda's method.[5] A mixture of the corresponding dicyano derivative **6c** (1.20 g, 1.84 mmol), 1,8-diazabicyclo[5,4,0]undec-7-ene (DBU; 0.42 g, 2.8 mmol), and anhydrous copper(II) chloride (40 mg, 0.30 mmol) in 15 ml of *n*-pentanol was refluxed for 48 h. After cooling to room temperature, the resulting mixture was poured into a large quantity of acetone and methanol, and cooled by immersion in an ice-water bath. The resulting dark blue precipitates were collected by filtration and washed with hot acetone. The sticky precipitates were dissolved in hot benzene to remove them from the paper. The solvent was evaporated to give dark blue liquid crystals. Purification was carried out by reprecipitation by adding acetone to a hot solution of the crude product in tetrahydrofuran to give 0.28 g of dark blue liquid crystals. Yield 23%. IR (KBr): 2920, 2850, 1610, 1510, 1470 cm^{-1}.

Each of the following $(C_nO)_8$M complexes could be prepared and purified in the same manner as the $(C_{12}O)_8$–Cu complex.

$(C_{12}O)_8$–Ni 2c. Dark green liquid crystals. Yield 14%. IR (KBr): 2920, 2850, 1610, 1510, 1470 cm^{-1}.

$(C_{10}O)_8$–Cu 1b. Dark green liquid crystals. Yield 10%. IR (KBr): 2920, 2850, 1610, 1510, 1470 cm^{-1}.

$(C_{10}O)_8$–Ni 2b. Dark green liquid crystals. Yield 10%. IR (KBr): 2920, 2850, 1610, 1510, 1470 cm^{-1}.

Each of the following $(C_nO)_{16}$–M complexes could be prepared in the same manner as the above-mentioned $(C_{12}O)_8$–Cu complex.

Table 2 Electronic absorption spectral data of $(C_nO)_8$–M (M = Cu **1**, M = Ni **2**) and $(C_nO)_{16}$–M (M = Cu **3**, M = Ni **4**) in $CHCl_3$

Complex	Concentration/mol l^{-1}	λ_{max}/nm (log[ε/dm^3 mol^{-1} cm^{-1}])					
1b: $(C_{10}O)_8$–Cu	1.15×10^{-5}	288 (4.79)	377 (5.06)	500 (4.52)	662 (4.77)		
2b: $(C_{10}O)_8$–Ni	1.10×10^{-5}	297 (4.83)	347 (4.92)	377 (4.92)	536 (4.54)	602 (4.64)	666 (5.33)
1c: $(C_{12}O)_8$–Cu	1.40×10^{-5}	290 (4.76)	377 (5.03)	500 (4.50)	662 (4.84)		
2c: $(C_{12}O)_8$–Ni	1.31×10^{-5}	296 (4.92)	378 (4.99)	492 (4.62)	602 (4.56)	653 (5.23)	
3a: $(C_8O)_{16}$–Ni	1.04×10^{-5}	276 (4.83)	351 (4.91)	377 (4.92)	541 (4.55)	601 (4.64)	666 (5.31)
4a: $(C_8O)_{16}$–Ni	0.96×10^{-5}	313 (4.92)	334 (4.91)	390 (4.88)	520 (4.53)	595 (4.59)	657 (5.28)
3b: $(C_{10}O)_{16}$–Cu	1.06×10^{-5}	276 (4.84)	346 (4.90)	377 (4.92)	542 (4.54)	602 (4.63)	666 (5.29)
4b: $(C_{10}O)_{16}$–Ni	0.97×10^{-5}	313 (4.93)	330 (4.92)	391 (4.88)	521 (4.54)	595 (4.59)	657 (5.27)
3c: $(C_{12}O)_{16}$–Cu	1.09×10^{-5}	276 (4.83)	347 (4.92)	377 (4.92)	536 (4.54)	602 (4.64)	666 (5.33)
4c: $(C_{12}O)_{16}$–Ni	1.14×10^{-5}	314 (4.89)	331 (4.87)	390 (4.83)	514 (4.49)	594 (4.53)	657 (5.22)

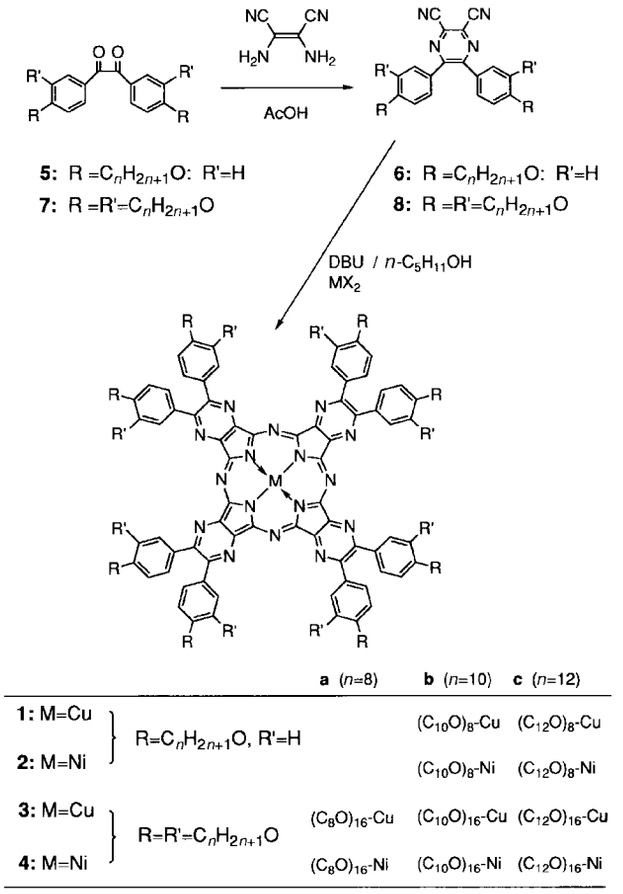

Fig. 1 Synthetic route to $(C_nO)_8$–M ($n=10$, 12; M = Cu **1**, M = Ni **2**) and $(C_nO)_{16}$–M ($n=8$, 10, 12; M = Cu **3**; M = Ni **4**). DBU = 1,8-diazabicyclo[5,4,0]undec-7-ene.

$(C_{12}O)_{16}$–Cu 3c. Purified by reprecipitation by adding acetone into a hot solution of the crude product in hexane to give dark blue liquid crystals. Yield 18%. IR (KBr): 2920, 2850, 1600, 1520, 1470 cm^{-1}.

Each of the other $(C_nO)_{16}$–M complexes was purified in the same manner as this $(C_{12}O)_{16}$–Cu complex.

$(C_{12}O)_{16}$–Ni 4c. Dark blue liquid crystals. Yield 14%. IR (KBr): 2920, 2850, 1600, 1520, 1470 cm^{-1}.

$(C_{10}O)_{16}$–Ni 4b. Dark blue liquid crystals. Yield 6%. IR (KBr): 2920, 2850, 1600, 1520, 1470 cm^{-1}.

$(C_8O)_{16}$–Cu 3a. Dark blue liquid crystals. Yield 8%. IR (KBr): 2930, 2860, 1600, 1520, 1470 cm^{-1}.

$(C_8O)_{16}$–Ni 4a. Dark blue liquid crystals. Yield 6%. IR (KBr): 2930, 2860, 1600, 1520, 1470 cm^{-1}.

3 Results and discussion

Discotic mesomorphism of $(C_nO)_8$–M (1, 2) and $(C_nO)_{16}$–M (3, 4)

Mesomorphism of $(C_nO)_8$–M (1, 2). The phase transitions of $(C_nO)_8$–M (**1**, **2**) are summarized in Table 3. Each of the pristine samples of $(C_nO)_8$–M (**1**, **2**) exhibits a tetragonal columnar (D_{tet}) mesophase from r.t. to *ca.* 150 °C. The X-ray powder diffraction patterns of $(C_{10}O)_8$–Cu **1** and $(C_{10}O)_8$–Ni **2** at 140 °C were compared with each other. The reflections in the low angle region could be assigned to a two-dimensional tetragonal lattice for each of the complexes. The $(C_{10}O)_8$–Cu **1** complex gave a relatively sharp reflection at $d=3.82$ Å, which could be assigned as an interdisk distance in the column. On the other hand, the $(C_{10}O)_8$–Ni **2** complex gave a broad and weak reflection at $d=ca.$ 3.7 Å, which corresponds to fluctuation of the interdisk distance in the column. Therefore, the D_{tet} phase

Table 3 Phase transition temperatures (T_t), enthalpy changes (ΔH) and X-ray data of $(C_nO)_8$–M ($n=10$, 12; M = Cu **1**, M = Ni **2**)

Complex	Phase	T_t/°C [ΔH/kJ mol^{-1}]	Phase[a]
1b: $(C_{10}O)_8$-Cu	$D_{tet.o}$ at 140°C, a=29.7 Å, h=3.82 Å	149[12.6]	D_{hd} at 180°C, a=34.6 Å; *ca.*230; 1st decomp.[b]; *ca.*300; 2nd decomp.
2b: $(C_{10}O)_8$-Ni	$D_{tet.d}$ at 140°C, a=30.3 Å, h=*ca.*3.7 Å	150[11.6]	D_{hd} at 180°C, a=37.2 Å; *ca.*210; 1st decomp.[b]; *ca.*250; 2nd decomp.
1c: $(C_{12}O)_8$-Cu	cooling; virgin $D_{tet.o}$ at 90°C, a=31.3 Å, h=3.77 Å	109[32.1]	$D_{rd}(C2/m)$ at 180°C, a=54.8 Å, b=43.4 Å; *ca.*230; 1st decomp.[b]; *ca.*300; 2nd decomp.
	D_{x1}	39[13.4]	D_{x2}
	D_{x2}	71[1.5]	$D_{rd}(C2/m)$
2c: $(C_{12}O)_8$-Ni	cooling; virgin $D_{tet.d}$ at 90°C, a=30.7 Å, h=*ca.*3.7 Å	109[26.5]	$D_{rd}(C2/m)$ at 150°C, a=53.3 Å, b=41.9 Å; *ca.*230; 1st decomp.[b]; *ca.*300; 2nd decomp.
	D_{x1}	34[14.9]	D_{x2}
	D_{x2}	68[1.4]	$D_{rd}(C2/m)$

[a]Phase nomenclature: D_{hd} = hexagonal disordered columnar mesophase, $D_{tet,o}$ = tetragonal ordered columnar mesophase, $D_{tet,d}$ = tetragonal disordered columnar mesophase and D_x = unidentified mesophase. [b]Ref. 3.

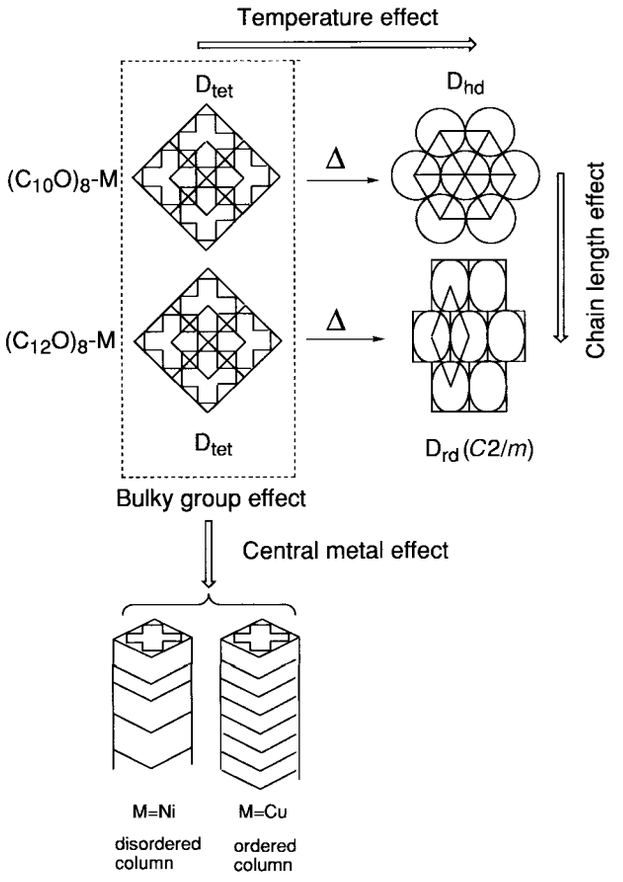

Fig. 2 Various effects on the liquid crystalline properties of $(C_nO)_8$–M (**1**, **2**).

of the copper complex was identified as an ordered columnar ($D_{tet.o}$) mesophase, whereas that of the nickel complex was identified as a disordered columnar mesophase ($D_{tet.d}$). The mesophases of $(C_{12}O)_8$–M (M = Cu, Ni) at r.t. could also similarly be identified. Hence, it is apparent that the $(C_nO)_8$–Cu complexes in the D_{tet} phase stack more regularly in columns than the $(C_nO)_8$–Ni complexes. More interestingly, on heating these D_{tet} phases change into a D_{hd} phase for the $(C_{10}O)_8$–M (M = Cu, Ni) derivatives, whereas they change into a D_{rd} (*C*2/*m*) phase for the $(C_{12}O)_8$–M (M = Cu, Ni) derivatives. Thus, the higher temperature mesophases depend not on the central metal but on the length of the peripheral chains. On further heating, each of the $(C_nO)_8$–M (**1**, **2**) derivatives decomposes by two steps. The first decomposition has also been observed for the octaphenyl-substituted Pc mesogenic derivatives.[3] Hence, we suppose that the decomposition may be due to a ring closure reaction between two neighboring phenyl groups at the *o*-positions. The second decomposition is usual degradation of the compounds.

When the $(C_{12}O)_8$–M (M = Cu, Ni) derivatives were cooled from the D_{rd} mesophase and heated again from r.t., they exhibited a different phase transition sequence, compared with the virgin samples. They showed two new metastable D_{x1} and D_{x2} phases (Table 3). These D_{x1} and D_{x2} mesophase structures could not be identified by X-ray diffraction studies, because they did not give clear reflections. Nevertheless, the metastable mesophases could be repeatedly obtained by cooling of the D_{rd} phase. On the other hand, when the D_{hd} phases of the $(C_{10}O)_8$–M (**1**, **2**) derivatives were cooled to r.t., the D_{hd} phases remained. Thus, all the $(C_{10}O)_8$–M (**1b**, **2b**) derivatives are easily supercooled.

As summarized in Fig. 2, the mesophases in the $(C_nO)_8$–M (**1**, **2**) derivatives are affected by the central metal, chain length, temperature and bulky phenyl groups. Steric hindrance of the bulky groups results in a D_{tet} phase (bulky group effect). These

Table 4 Phase transition temperatures (T_t), enthalpy changes (ΔH) and X-ray data of $(C_nO)_{16}M$ (M = Cu **3**, M = Ni **4**)

Complex	Phase	T_t/°C[ΔH/kJ mol^{-1}]			Phase[a]
3a: $(C_8O)_{16}$-Cu	X	-29 ~39 → $D_{rd1}(C2/m)$ at 200°C, *a*=63.7 Å, *b*=28.1 Å	247[13.8] → $D_{rd2}(C2/m)$ at 250°C, *a*=62.6 Å, *b*=27.9 Å	323 →	decomp.?
4a: $(C_8O)_{16}$-Ni	X	-41 ~11 → $D_{rd1}(C2/m)$ at 150°C, *a*=60.8 Å, *b*=26.3 Å	226[8.3] → $D_{rd2}(C2/m)$ at 280°C, *a*=62.0 Å, *b*=26.4 Å; D_{x1} 245	324 →	decomp.?
3b: $(C_{10}O)_{16}$-Cu	X	-13 ~ 29 → $D_{rd1}(C2/m)$ at 150°C, *a*=69.7 Å, *b*=29.9 Å	221[8.0] → $D_{rd2}(C2/m)$ at 245°C, *a*=68.8 Å, *b*=30.0 Å	281[13.1] → I.L.[b]	
4b: $(C_{10}O)_{16}$-Ni	D_{hd} at r.t., *a*=36.0 Å	41[64.6] → $D_{rd1}(C2/m)$ at 200°C, *a*=69.7 Å, *b*=30.1 Å	214[5.4] → $D_{rd2}(C2/m)$ at 250°C, *a*=68.7 Å, *b*=30.0 Å	269[9.5] → I.L.[b]	
3c: $(C_{12}O)_{16}$-Cu D_{x2} 14 →	D_{hd} at r.t., *a*=34.8 Å	44[184.8] → $D_{rd1}(C2/m)$ at 150°C, *a*=71.7 Å, *b*=35.8 Å	194[7.3] → $D_{rd2}(C2/m)$ at 210°C, *a*=72.5 Å, *b*=36.2 Å	241[11.3] → I.L.[b] *ca.*320 →	decomp.
4c: $(C_{12}O)_{16}$Ni	D_{hd} at r.t., *a*=36.3 Å	40[148.9] → $D_{rd1}(C2/m)$ at 200°C, *a*=70.8 Å, *b*=32.6 Å	206[7.3] →	I.L.[b] *ca.*320 →	decomp.

[a]Phase nomenclature: D_{hd} = hexagonal disordered columnar mesophase, D_{rd} = rectangular disordered columnar mesophase, X = several unidentified transitions were observed, D_x = unidentified mesophase and I.L. = isotropic liquid. [b]Gradual decomposition during several heating and cooling cycles ⩽285 °C.

D_{tet} mesophases have an ordered columnar structure and a disordered columnar structure for copper and nickel, respectively (central metal effect). Moreover, the D_{tet} mesophases change into the D_{hd} phase for the $(C_{10}O)_8$–M (M = Cu, Ni) derivatives, and into D_{rd} (*C2/m*) for the $(C_{12}O)_8$–M (M = Cu, Ni) derivatives, respectively (temperature and chain length effects).

Mesomorphism of $(C_nO)_{16}$–M (3, 4). The phase transitions of $(C_nO)_{16}$–M (**3**, **4**) are summarized in Table 4. $(C_{10}O)_{16}$–Ni (**4b**), $(C_{12}O)_{16}$–Cu (**3c**) and $(C_{12}O)_{16}$–Ni (**4c**) gave a D_{hd} phase at r.t. $(C_8O)_{16}$–Cu (**3a**), $(C_8O)_{16}$–Ni (**4a**) and $(C_{10}O)_{16}$–Cu (**3b**) exhibited complicated phase transitions at low temperatures below r.t. For the DSC measurements, they showed several very complicated peaks which were not reproducible. Therefore, we noted only the start and end temperatures of these peaks and denoted them as an X-phase in Table 4. Very interestingly, each of the $(C_nO)_{16}$–M (**3**, **4**) derivatives except for $(C_{12}O)_{16}$–Ni (**4**) exhibits a $D_{rd1} \rightarrow D_{rd2}$ phase transition. Each of the D_{rd} phases has *C2/m* symmetry, which was established from the extinction rules of X-ray reflections for D_{rd} phases.[6] These two D_{rd} (*C2/m*) phases repeatedly appeared for the DSC measurements. However, the origin of the phase transition from D_{rd1} (*C2/m*) to D_{rd2} (*C2/m*) is not clear at this present time.

$(C_{10}O)_{16}$–M (M = Cu, Ni) (**3b**, **4b**) and $(C_{12}O)_{16}$–M (M = Cu, Ni) (**3c**, **4c**) gave isotropic liquids, whereas $(C_8O)_{16}$–M (M = Cu, Ni) (**3a**, **3b**) did not give an isotropic liquid (I.L.) until 300 °C. The endothermic peaks observed at 323 °C and 324 °C by DCS measurements could not be identified by our polarizing microscope because of the instrumental limit of the heating plate. During several heating–cooling cycles even below 285 °C, all the $(C_nO)_{16}$–M (M = Cu, Ni) derivatives gradually decomposed. This decomposition may be attributable to the same ring closure reaction between adjacent phenyl groups as for the $(C_nO)_8$–M derivatives, mentioned above. This gradual decomposition by ring closure was observed by the polarizing microscope. For example, when one of the $(C_{12}O)_{16}$–M (M = Cu, Ni) derivatives was held at *ca.* 285 °C for several hours, a birefringent rigid crystalline area appeared from the I.L. and gradually spread over the whole area. This crystal did not melt into an I.L. The same solidification was not observed for the analogous Pc derivatives, $[(C_nO)_2Ph]_8PcCu$,[7] although they have the same octakis(dialkoxyphenyl) substituents as the present $(C_nO)_{16}$–M (M = Cu, Ni) derivatives.

Thus, the $(C_nO)_{16}$–M (Cu, Ni) derivatives gave a higher symmetry D_{hd} phase at lower temperatures and a lower symmetry D_{rd} phase at higher temperatures. It is very interesting that this sequence is quite opposite to the general phase transition sequence: a higher symmetry phase usually appears at higher temperatures.[8]

To reveal this unique mesomorphism, the electronic absorption spectra of $(C_nO)_8$–M (**1**, **2**) and $(C_nO)_{16}$–M (**3**, **4**) both in solution and as mesophase thin films were recorded.

Electronic absorption spectra of $(C_nO)_8$–M (1, 2) and $(C_nO)_{16}$–M (3, 4)

Electronic absorption spectra of $(C_{12}O)_8$–M (**1c**, **2c**) and $(C_{12}O)_{16}$–M (**3c**, **4c**) in $CHCl_3$ are summarized in Fig. 3, and the spectral data of all the derivatives are listed in Table 2. As can be seen from Fig. 3b–d, $(C_{12}O)_8$–Ni (**2c**) and $(C_{12}O)_{16}$–M (**3c**, **4c**) show spectra typical of monomeric Pc analogues.[9] A sharp peak of the Q band around 660 nm and a broad peak of the Soret band around 390 nm could be observed. On the other hand, the Q band of $(C_{12}O)_8$–Cu (**1c**) is broader and weaker (Fig. 3a) than those of the other complexes (**2c**, **3c**, **4c**). This means that only $(C_{12}O)_8$–Cu (**1c**) tends to aggregate more in $CHCl_3$, even though it is present at a similar concentration (*ca.* 1×10^{-5} mol l^{-1}) to the other complexes. As illustrated in Fig. 4b and c, $(C_{10}O)_8$–Cu (**1b**) also shows high aggregation in $CHCl_3$, at a concentration of *ca.* 1×10^{-5} mol l^{-1}. The spectrum observed at much lower concentration (1.1×10^{-7} mol l^{-1}) shows a sharp Q band, and this absor-

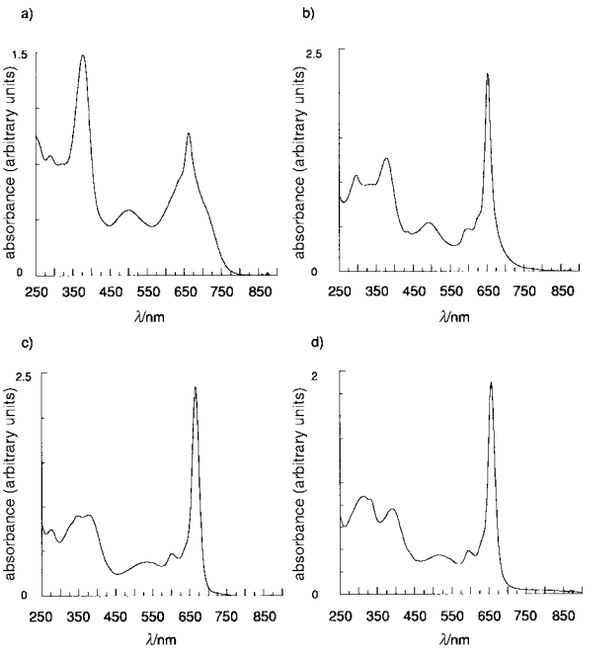

Fig. 3 Electronic absorption spectra of the $CHCl_3$ solutions: a) $(C_{12}O)_8$–Cu (1.40×10^{-5} mol l^{-1}), b) $(C_{12}O)_8$–Ni (1.31×10^{-5} mol l^{-1}), c) $(C_{12}O)_{16}$–Cu (1.09×10^{-5} mol l^{-1}), d) $(C_{12}O)_{16}$–Ni (1.14×10^{-5} mol l^{-1}).

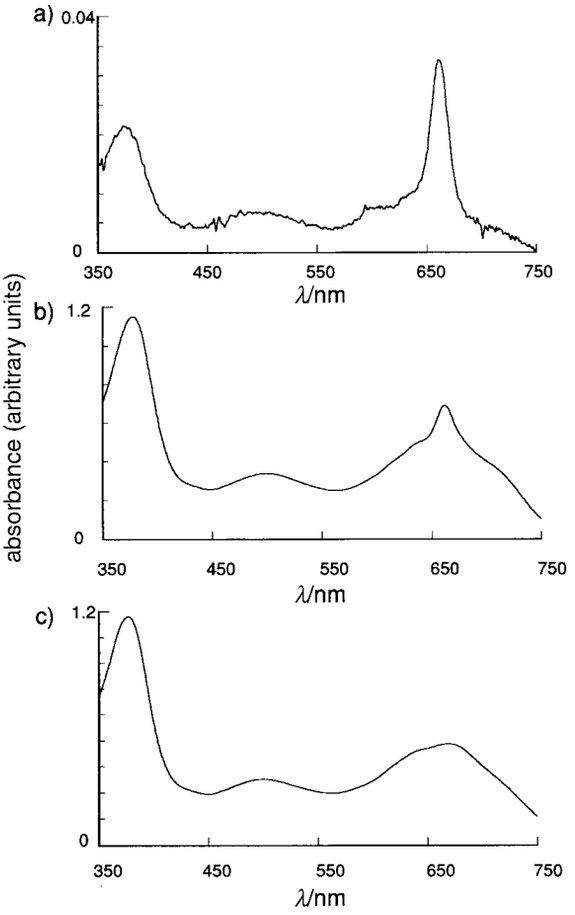

Fig. 4 Electronic absorption spectra of $(C_{10}O)_8$–Cu in $CHCl_3$ at various concentrations; a) $c = = 1.105 \times 10^{-7}$ mol l^{-1}, b) $c = 0.995 \times 10^{-5}$ mol l^{-1}, c) $c = 1.062 \times 10^{-5}$ mol l^{-1}.

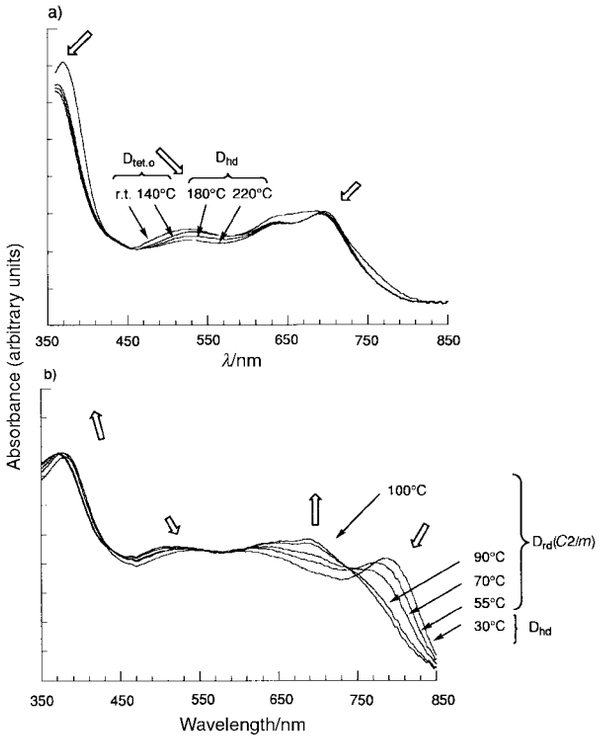

Fig. 5 Temperature-dependent electronic absorption spectra of thin films of a) $(C_{10}O)_8$–Cu and b) $(C_{12}O)_{16}$–Cu. The thin films were prepared by casting.

bance is bigger than that of the Soret band (Fig. 4a). From these results, it is apparent that the $(C_nO)_8$–Cu (**1b**, **c**) derivatives more easily aggregate than the other $(C_nO)_8$–Ni (**2b**, **c**) and $(C_nO)_{16}$–M (**3**, **4**) derivatives in $CHCl_3$.

Compared with the Q band and Soret bands of the core Pz derivative without octaphenyl groups in the periphery, both the Q and Soret bands of the present $(C_nO)_8$–M (**1**, **2**) and $(C_nO)_{16}$–M (**3**, **4**) derivatives are located at much longer wavelengths (shifted about 30 nm) and their absorption coefficients (ε) are about twice as large.[9] Such phenomena have been reported in other compounds. For example, tetra-*tert*-butylated magnesium tetraazaporphyrin shows Q_{0-0} and Soret bands at 592 nm and 335 nm, while octaphenylated magnesium tetraazaporphyrin shows these at 636 and 378 nm, respectively, in pyridine. The ε values of the latter are about 3–6 times larger than those of the former.[10] Interestingly, an absorption peak at *ca.* 500 nm could be observed for all the present Pz derivatives, although it is not seen for the core Pz derivative. Although not yet rationalized, this peak is frequently observed when a number of phenyl groups are attached to porphyrins and/or phthalocyanines.[10]

3.3 Relationship between liquid crystalline properties and aggregation in *n*-hexane of $(C_nO)_8$–M (1, 2)

As mentioned above, the $(C_nO)_8$–Cu (**1**) complexes have stronger molecular interactions and aggregate more in chloroform than the $(C_nO)_8$–Ni (**2**) complexes. This may correspond to the stacking order in columnar mesophases in the absence of solvent. Actually, the $(C_nO)_8$–Cu complexes give an ordered

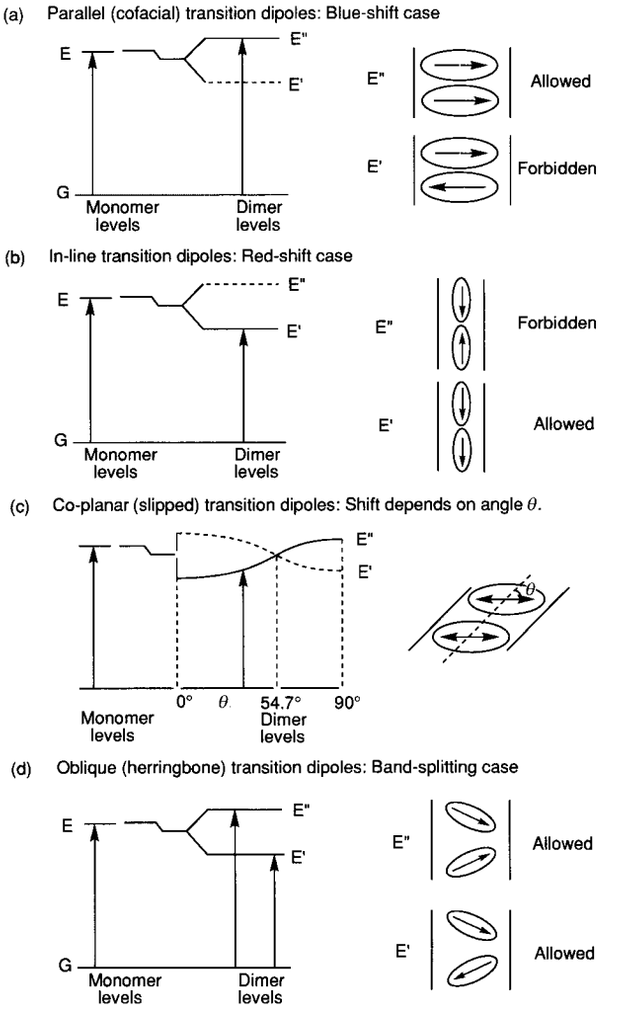

Fig. 6 Exciton energy diagrams for various dimers.

$D_{tet.o}$ columnar mesophase, whereas the $(C_nO)_8$–Ni complexes give a disordered $D_{tet.d}$ columnar mesophase (Table 3).

3.4 Electronic absorption spectra of thin films of $(C_nO)_8$–M (1, 2) and $(C_nO)_{16}$–M (3, 4)

Fig. 5 shows electronic absorption spectra of cast thin films of $(C_{10}O)_8$–Cu (**1b**) and $(C_{12}O)_{16}$–Cu (**3c**) at various temperatures. $(C_{10}O)_8$–Cu (**1b**) shows very little change with increasing temperature (Fig. 5a). The Q-band and Soret band are slightly blue-shifted and the band at *ca.* 500 nm is slightly red-shifted, as indicated by open arrows in this figure. On the other hand, $(C_{12}O)_{16}$–Cu (**3c**) shows two Q bands which are split widely into peaks at *ca.* 620 nm and *ca.* 800 nm (Fig. 5b). Such a wide separation has been reported previously for long-chain-substituted phthalocyanines[11] and the X-polymorph of non-substituted phthalocyanine upon forming dimers.[12] As can be seen from Fig. 5b, the intensity of the Q-band of the thin film at *ca.* 800 nm gradually decreased and blue-shifted with increasing temperature. Finally, the band at *ca.* 800 nm disappeared and a new band at 680 nm appeared. Similar behavior has been reported previously, and two different interpretations have

Table 5 Vapor pressure osmometric data for $(C_{12}O)_{16}$–Cu ($M^{theor}=4141.95$)

Solvent	Concentration/mol l^{-1}	Observed molecular weight, M^{obs}	Number of molecules in an aggregate ($n=M^{obs}/M^{theor}$)
n-Hexane (35 °C)	1.62×10^{-4}	7274	1.8 (≈2)
n-Hexane (35 °C)	1.01×10^{-4}	6979	1.7 (≈2)
n-Hexane (35 °C)	0.42×10^{-4}	8832	2.1 (≈2)
$CHCl_3$ (35 °C)	1.21×10^{-4}	4401	1.1 (≈1)

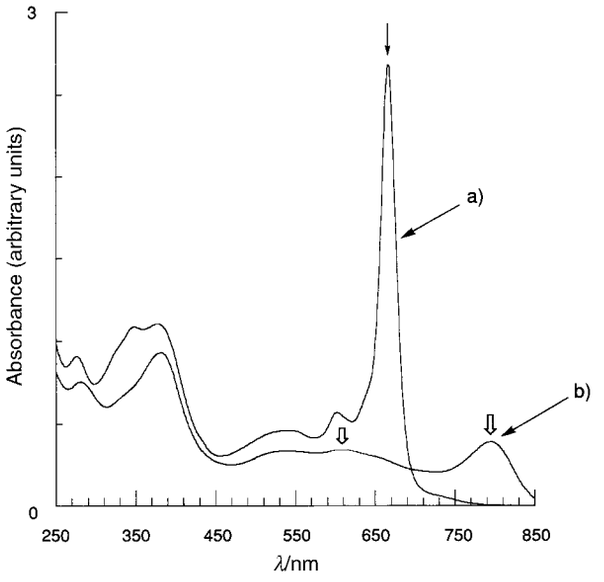

Fig. 7 Electronic absorption spectra of $(C_{12}O)_{16}$–Cu: a) the $CHCl_3$ solution (1.30×10^{-5} mol l^{-1}), and b) the *n*-hexane solution (1.18×10^{-5} mol l^{-1}).

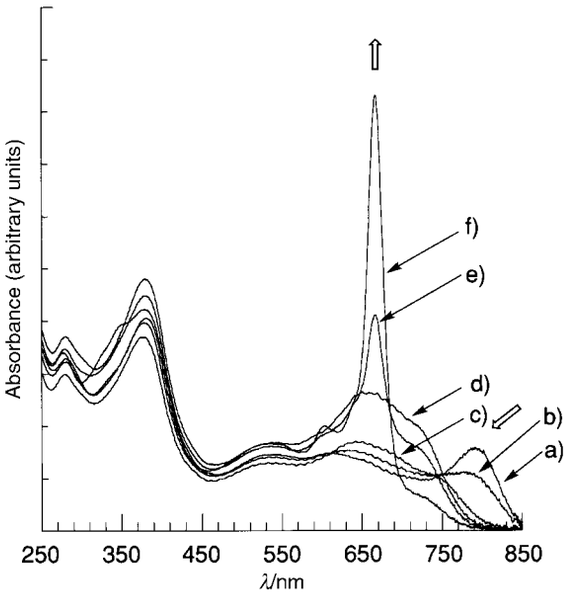

Fig. 8 Electronic absorption spectra of $(C_{12}O)_{16}$–Cu in $CHCl_3$–*n*-hexane mixtures. $CHCl_3$: *n*-hexane ratio: a) 3 : 100 (v/v), b) 4 : 100 (v/v), c) 7.5 : 100 (v/v), d) 7 : 100 (v/v), e) 150 : 100 (v/v), and f) 100 : 3 (v/v).

been suggested.[11] One of them is that such a spectral change is attributable to a change from dimers to monomers.[11b] Another interpretation is that the molecular stacking changes from herringbone to parallel.[11c] As mentioned above, the present $(C_{12}O)_{16}$–Cu complex gives a D_{hd} mesophase at r.t. and the molecules stack to form columns which are arranged in a 2D-hexagonal lattice. According to the first interpretation, the $(C_{12}O)_{16}$–Cu molecules may form dimers, which stack to form columns. Since the present Pz molecules are substituted by phenyl groups (Fig. 1), the Pz cores may rotate through 45° to form the dimers. From the exciton coupling theory[13] (Fig. 6), none of the parallel, in-line and slipped dimers show such Q-band splitting; only the oblique dimer gives such a band-splitting. Nevertheless, parallel dimers of the core Pz molecules also give Q-band splitting in one case: it was reported that a sandwich lutetium double-decker of Pz gave a wide Q-band splitting.[14] This may be ascribed to a partition of angular momentum, so that the magnetic circular dichromism (MCD) spectrum of the split Q-bands shows Faraday A term dispersions. Hence, in this case we could not explain the Q-band splitting from pure exciton coupling theory. To clarify the wide splitting of Q-bands for the cast thin film in the mesophase of the present $(C_{12}O)_{16}$–Cu complex, electronic absorption spectra of *n*-hexane and chloroform solutions were recorded (Fig. 7). The spectrum of $(C_{12}O)_{16}$–Cu in chloroform is typical of metal phthalocyanines having D_{4h} symmetry and the Q-band is located at 666 nm, as shown in Fig. 7a. On the other hand, the spectrum in *n*-hexane shows wide-split Q-bands at 661 nm and 798 nm, similarly to the thin film at r.t. (Fig. 5b). Generally, the aggregation band of phthalocyanines appears at longer wavelength than the Q-band of monomers.[15] As far as we know, such wide-split Q-bands have been reported for the spectra of Pc derivatives in solid states,[11,15] but have never been reported for the spectra in solution. The wide-split Q-bands could be observed in the solid state for an X-polymorph of phthalocyanine. In this X-polymorph, the phthalocyanine molecules form dimers. Therefore, the present $(C_{12}O)_{16}$–Cu complex may form dimers in *n*-hexane solution. The number of molecules in an aggregate in the solutions was determined by using the vapor pressure osmometry (VPO) technique. As listed in Table 5, the number of molecules in an aggregate is nearly equal to one in chloroform solution, whereas the number is nearly equal to two in *n*-hexane solution. Thus, the $(C_{12}O)_{16}$–Cu complex forms dimers in *n*-hexane solution.

When chloroform was gradually added to the *n*-hexane solution, the wide-split Q-bands gradually converged into a single peak, as shown in Fig. 8. This gradual change upon the addition of chloroform corresponds well with the gradual spectral change upon heating of the thin film, as already shown in Fig. 5b. To clarify the dimer structure, MCD spectra were recorded for *n*-hexane and chloroform solutions. Fig. 9 shows the MCD spectra together with the electronic absorption

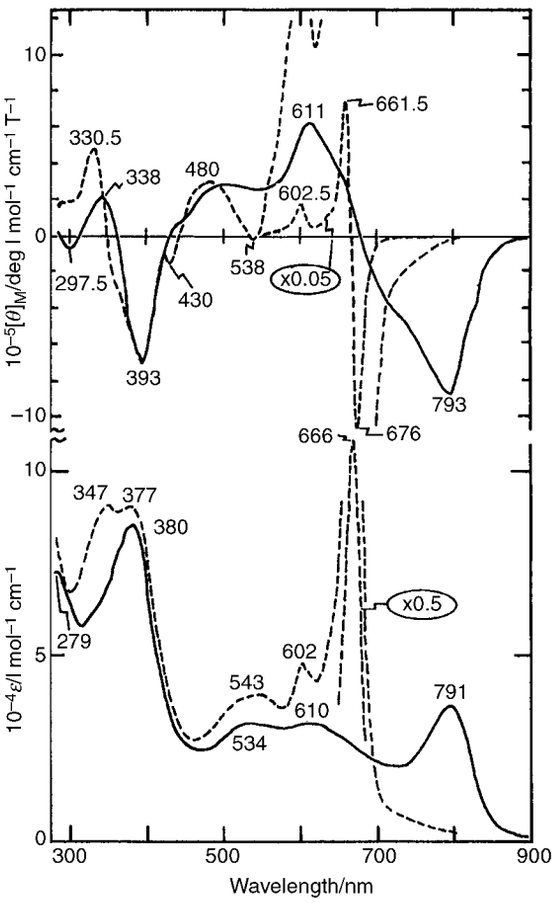

Fig. 9 Magnetic circular dichromism (a) and electronic absorption spectra (b) of $(C_{12}O)_{16}$–Cu in *n*-hexane (—) and $CHCl_3$ (---).

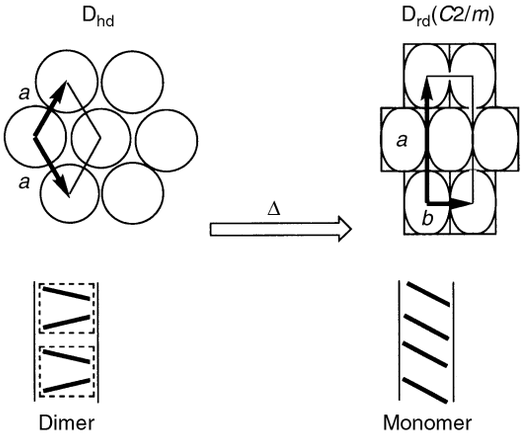

Fig. 10 Schematic models of the molecular arrangement of $(C_{12}O)_{16}$–Cu in D_{hd} and D_{rd} mesophases.

spectra. As has been proven by the VPO measurements, the $(C_{12}O)_{16}$–Cu complex exists as a monomer and dimer in chloroform and *n*-hexane, respectively. Both the electronic absorption and MCD spectra in chloroform have characteristics of phthalocyanine analogues with D_{4h} symmetry.[16] That is, a Faraday A term appears, corresponding to the Q_{0-0} band, indicating that the excited states are degenerate. The absorption spectrum in *n*-hexane is quite different from that in chloroform, displaying a much weaker and split Q-band. Faraday B terms appear in the MCD spectrum, corresponding to the positions of the peaks at *ca.* 611 nm and 793 nm of the electronic absorption spectrum. From the dispersion B terms, these adjacent transitions are judged to be interacting.[17] This is clear evidence that two bands at 611 nm and 793 nm in *n*-hexane originate from exciton coupling of the Q band at 666 nm in chloroform, and that the $(C_{12}O)_{16}$–Cu complexes aggregate into oblique dimers in *n*-hexane.

3.5 Models of molecular arrangement of $(C_nO)_{16}$–M in D_{hd} and D_{rd} mesophases

The spectrum of $(C_{12}O)_{16}$–Cu in *n*-hexane is the same as that of the thin film in the D_{hd} mesophase at r.t. (Fig. 5b and 7b). Hence, the D_{hd} $(C_{12}O)_{16}$–Cu complex at r.t. forms oblique dimers stacking to form a 2-D hexagonal columnar structure, as illustrated in Fig. 10. It is noteworthy that these phthalocyanine disks are arranged not co-facially but obliquely in this D_{hd} mesophase, although disks in D_h mesophases have been commonly believed to stack co-facially. The spectrum of the thin film in the D_{rd} mesophase at higher temperatures shows a non-splitting Q-band (Fig. 5b). Hence, the dimers of the D_{hd} $(C_{12}O)_{16}$–Cu complex may be broken into monomers and stack in slipped form in the D_{rd} mesophase, as illustrated in Fig. 10. These columns are packed into a 2D-rectangular lattice having *C*2/*m* symmetry, as described above. In general, molecules in rectangular columnar mesophases stack in slipped form. This is compatible with the present spectral results.

Thus, dimerization of the $(C_nO)_{16}$–M complexes (**3**, **4**) results in such a unique phase transition sequence from D_{hd} to D_{rd}. This is quite opposite to the general tendency for higher symmetry mesophases to appear at higher temperatures.

4 Conclusion

The mesomorphism of $(C_nO)_8$–M complexes (**1**, **2**) is very sensitive to changes in the central metal and chain length. The $(C_nO)_{16}$–M complexes (**3**, **4**) exhibit a higher symmetry mesophase, D_{hd}, at *lower* temperatures, contrary to general tendency: higher symmetry mesophases usually appear at *higher* temperatures. It was revealed from the electronic absorption spectra, MCD spectra and VPO measurements that such a unique phase sequence is attributable to dimerization.

References

1 K. Ohta, Y. Inagaki-Oka, H. Hasebe and I. Yamamoto, *Polyhedron Symposium in Print*, in press.
2 (*a*) H. Ema, Master Thesis, Shinshu University, Ueda, Japan, 1988, ch. 7; (*b*) H. Hasebe, Master Thesis, Shinshu University, Ueda, Japan, 1991, ch. 5
3 K. Ohta, T. Watanabe, S. Tanaka, T. Fujimoto, I. Yamamoto, P. Bassoul, N. Kucharczyk and J. Simon, *Liq. Cryst.*, 1991, **10**, 357.
4 K. Kanakarajan and A. W. Czarnik, *J. Org. Chem.*, 1986, **51**, 5241.
5 H. Tomoda, S. Saito, S. Ogawa and S. Shiraishi, *Chem. Lett.*, 1980, 1277.
6 T. Komatsu, K. Ohta, T. Watanabe, H. Ikemoto, T. Fujimoto and I. Yamamoto, *J. Mater. Chem.,* 1994, **4**, 537; see Table 2 and Fig. 2 of this reference.
7 K. Ohta, S. Azumane, T. Watanabe, S. Tsukada and I. Yamamoto, *Appl. Organomet. Chem.*, 1996, **10**, 623.
8 C. Destrade, P. Foucher, H. Gasparoux, H.-T. Nguyen, A. M. Levelut and J. Malthête, *Mol. Cryst. Liq. Cryst.*, 1984, **106**, 121.
9 N. Kobayashi, *Phthalocyanines—Properties and Applications*, ed. C. C. Leznoff and A. B. P. Lever, VCH, Weinheim, New York, 1993, vol. II, ch. 3.
10 (*a*) N. Kobayashi, R. Kondo, S. Nakajima and T. Osa, *J. Am. Chem. Soc.*, 1990, **112**, 9640; (*b*) N. Kobayashi, T. Ashida and T. Osa, *Chem. Lett.*, 1992, 2031.
11 (*a*) M. J. Cook, N. B. McKeown, A. J. Thomson, K. J. Harrison, R. M. Richardson, A. N. Davies and S. J. Roser, *Chem. Mater.*, 1989, **1**, 287; (*b*) Y. Suda, K. Shigehara, A. Yamada, H. Matsuda, S. Okada, A. Masaki and H. Nakanishi, *Proc. SPIE—Int. Soc. Opt. Eng.*, 1991, **1560**, 75; (*c*) D. Markoisti, I. Lécuyer and J. Simon, *J. Phys. Chem.*, 1991, **95**, 3620; (*d*) W. J. Scheutte, M. Sluyters-Rehbach and J. H. Sluyters, *J. Phys. Chem.*, 1993, **97**, 6069.
12 (*a*) J. H. Sharp and M. Lardon, *J. Phys. Chem.*, 1968, **72**, 3230; (*b*) J. H. Sharp and M. Abkowitz, *J. Phys. Chem.*, 1973, **77**, 477.
13 M. Kasha, H. R. Rawls and M. A. El-Bayoumi, *Pure Appl. Chem.*, 1965, **11**, 371.
14 N. Kobayashi, J. Rizhen, S. Nakajima, T. Osa and H. Hino, *Chem. Lett.*, 1993, 185.
15 (*a*) K. Bernauer and S. Fallab, *Helv. Chim. Acta*, 1961, **44**, 1287; (*b*) N. S. Hush and I. S. Woolsey, *Mol. Phys.*, 1971, **21**, 465; (*c*) N. Kobayashi and A. B. P. Lever, *J. Am. Chem. Soc.*, 1987, **109**, 7433.
16 M. J. Stillman and T. Nyokong, *Phthalocyanines—Properties and Applications*, ed. C. C. Leznoff and A. B. P. Lever, VCH, Weinheim, New York, 1989, ch. 3.
17 A. Tajiri and J. Winkler, *Z. Naturforsch., Teil A*, 1983, **38**, 1263.

Paper 9/05538J